JOURNAL OF PROPULSION AND POWER
Vol. 25, No. 1, January–February 2009

Effects of Floating-Ring Seal Clearance on the Pump Performance for Turbopumps

Chang-Ho Choi,* Jun-Gu Noh,† Dae-Jin Kim,† Soon-Sam Hong,‡ and Jinhan Kim§
Korea Aerospace Research Institute, Daejeon 305-333, Republic of Korea

DOI: 10.2514/1.36806

Pumps for a turbopump generally operate under high rotational speeds and large-head-rise conditions. Therefore, reliability is a prime design requirement. Floating-ring seals are frequently employed in a turbopump because of robustness despite relatively high leakage losses. A number of studies have been performed on the floating-ring seal itself, but the effects of the floating-ring seal on the performance of the whole pump are not widely studied, in spite of their importance. The effects of floating-ring seal clearance on the hydraulic and suction performances of a pump are investigated by both experimental and computational methods in the present study. The experimental results showed that the head rise and the efficiency increased as the floating-ring seal clearance decreased. The results also showed that the leakage flow injected into the inducer inlet enhanced the suction performance of the pump by diminishing the size of the backflows. The strength of the backflow becomes weak as the injected leakage flow at the inducer inlet prevents the flow from prerotation.

Nomenclature

A_{cl}	=	floating-ring seal clearance area
A_1	=	inducer inlet area
c	=	floating-ring seal clearance
D	=	floating-ring seal diameter
f	=	friction coefficient
g	=	gravitational acceleration, 9.8 m/s^2
L_c	=	floating-ring seal clearance length
r^*	=	dimensionless radius, $(r - r_h)/(r_s - r_h)$
Q	=	volume flow rate
T	=	torque
U	=	speed of the blade
v_z	=	flow axial velocity
z	=	axial coordinate
η	=	efficiency, $Q(p_{2t} - p_{1t})/(T\omega)$
η_L	=	volumetric efficiency, $Q_d/(Q_d + \Sigma Q_L)$
σ	=	cavitation number, $2(p_{1t} - p_v)/(\rho U_{1t}^2)$
ϕ	=	flow coefficient, $Q/(A_1 U_{1t})$
ψ	=	head coefficient, $2(p_{2t} - p_{1t})/(\rho U_{2t}^2)$
ω	=	pump rotational speed, rad/s

Subscripts

d	=	design
h	=	hub
L	=	leakage
s	=	shroud
t	=	tip or total
v	=	vapor
1	=	inducer inlet
2	=	pump outlet or impeller outlet

Received 23 January 2008; accepted for publication 30 September 2008.

*Senior Researcher, Turbopump Department, 45 Eoeun-Dong, Yuseong. Member AIAA.
†Research Engineer, Turbopump Department, 45 Eoeun-Dong, Yuseong.
‡Senior Researcher, Turbopump Department, 45 Eoeun-Dong, Yuseong.
§Head of Department, Turbopump Department, 45 Eoeun-Dong, Yuseong.

I. Introduction

MODERN liquid-rocket-propulsion systems generally employ two types of propellant-feed cycles: pressure-feed and turbopump-feed cycles. Because high efficiency and thrust in the propulsion cycle entails high chamber pressure, a pressure-feed cycle is less desirable for highly loaded propulsion systems due to its excessively high tank pressure requirement. On the other hand, a turbopump-feed cycle leads to a comparatively lower system weight and improved performance [1,2]. Therefore, turbopump systems, which pressurize liquid oxidizers and fuels, are frequently employed to achieve a high specific impulse.

A typical pump system for a turbopump consists of an inducer, impeller, volute, and seal passages. An inducer is employed in a modern rocket feed system because it allows a turbopump system to operate at a high speed with low inlet pressures to minimize the weight and the size of the system [3]. Cavitation performance can be improved by installing an inducer to the pump, thus increasing the operational speed of the pump. With the aid of the anticavitation function of the inducer, a centrifugal impeller can pump low-pressure propellants to high discharge pressures without cavitation breakdown [3–5]. Therefore, most recent research on turbopumps has focused on inducer flow phenomena such as backflows at the inducer inlet and cavitation instabilities [6,7].

Noncontact seals such as the labyrinth and floating ring are generally preferred in turbopump applications, in which high reliability is an important requirement in liquid-oxygen and high-rotational-speed environments [1]. Between these two noncontact seals, floating-ring seals (FRSs) are frequently employed in a turbopump because the FRS is rotordynamically robust and simple in design. The FRS is adopted in the present study because the Korea Aerospace Research Institute is currently developing a 30-t-class demonstrator engine that employs a turbopump with an FRS [8]. Figure 1 shows a simplified configuration of the present pump with seal passages that are located on the front and rear sides of the impeller shoulders. The leakage flow from the front seal is injected (or recirculated) to the inducer/impeller interface, and the leakage flow from the rear seal is injected to the inducer inlet along the bypass pipe after cooling the rear bearing. More precisely, the leakage flow from the rear seal is injected through the axisymmetrically located injection holes.

As mentioned earlier, most studies have been focused on the flow phenomena around the inducer and there have been many studies on the FRS itself [9–12], but the effects of the FRS on the performance of the whole pump are not widely studied in spite of their importance. The effects of FRS clearance on the hydraulic and suction performances of a pump are investigated by both experimental and

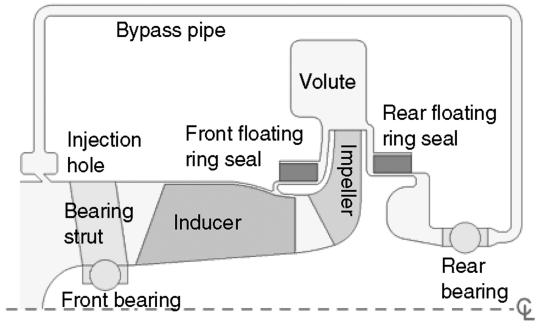

Fig. 1 Layout of the present pump.

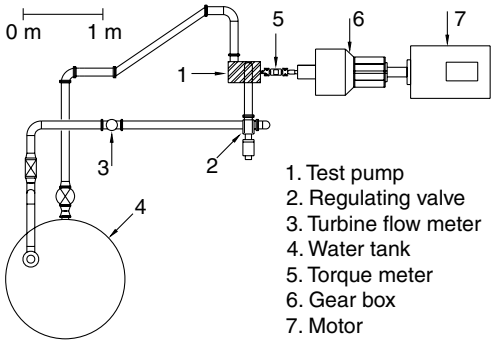

Fig. 2 Plane view of the pump test rig.

computational methods in the present study. The hydraulic and suction performances of the pump were measured with three different floating-ring seal clearances. A three-dimensional computational fluid dynamics (CFD) method was adopted to simulate the interaction between the injected leakage flow and the main flow around the inducer inlet. Furthermore, a one-dimensional (1-D) correlation was used to estimate the leakage flow rate, which could not be measured in the experiments.

II. Experimental Setup and Pump Design

Hydraulic and cavitation tests for the pump are conducted in a pump test facility in which the pump is driven by an electric motor. The working fluid is water at room temperature, and measurement parameters include static pressure, flow rate, rotational speed, and torque. The facility is composed of a water tank, an electric motor, a gear box, a torque meter, and a turbine-type flow meter. The water tank has a volume of 3.0 m^3 and its pressure can be adjusted by using a vacuum pump and compressed air. The maximum speed of the pump test is 20,000 rpm, and the maximum power of the electric motor is 320 kW. An outline of the closed-loop test facility is shown in Fig. 2, in which the test pump, the torque meter, and the gear box are arranged from left to right [13]. The uncertainties of measured values for head coefficient, efficiency, and flow coefficient are estimated to be 0.2, 0.5, and 0.4%, respectively.

Table 1 summarizes the design characteristics of the pump under consideration. The only difference among the three cases is the FRS radial clearance. The FRS radial clearance decreases from case 1 to case 3. The FRS radial clearance in case 3 is half of that of case 1. The experiments were conducted at speeds of 8000 to 9000 rpm. The pump showed stable operation for case 3, although the FRS radial clearance was small.

III. Results and Discussions

Figure 3 shows measured head and efficiency distributions of the pump. The head and efficiency of the pump increase as the FRS clearance decreases due to the decrease of the leakage flow through the FRS (i.e., the increase of the volumetric efficiency). The efficiency increases as the flow rate is increased, because the pump inlet is designed to have a larger diameter than hydraulically optimal to enhance the suction performance of the pump.

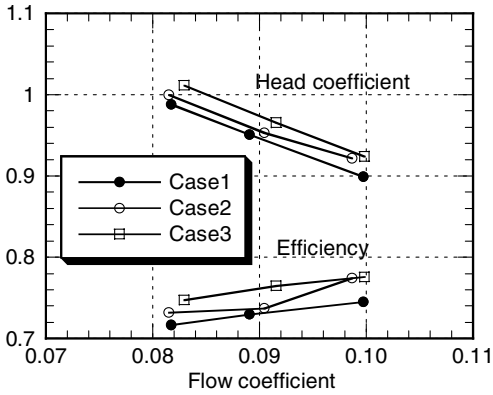

Fig. 3 Measured pump performance curves.

Table 2 summarizes the measured head coefficient and efficiency at the design flow rate in comparison with the 1-D calculation and CFD results. The estimated volumetric efficiencies are also presented in Table 2. The volumetric efficiency was not measured in the experiments. The computational result was obtained from a previous study [14]. The head rise of case 3 is about 3% higher than that of case 1, showing that the FRS clearance has a significant effect on the performance of the pump.

An in-house 1-D correlation method, which was originally developed to design pumps, was used to calculate the leakage flow rate through the FRS, because it was difficult to measure the leakage flow rate accurately in the experiments. The present 1-D method employs theoretical head-rise equations, slip-velocity theories, and loss equations with empirical correlations, which are typical in pump designs [15,16]. The computation was conducted only for case 1 and included all the pump components such as inducer, impeller, volute, and seal passages to evaluate the pump performance accurately. The computational results agree well with the experimental results, suggesting that the computational results can be used to evaluate the accuracy of the 1-D method for calculating the leakage flow rate. The head and efficiency of the 1-D results are different from those of the experiments by less than 4%, and the volumetric efficiency (leakage flow rate) of the 1-D results shows a difference compared with those

Table 1 Pump design specifications

Parameters	Case 1	Case 2	Case 3
Inducer design flow coefficient ϕ	0.09	0.09	0.09
Inducer inlet hub to tip diameter ratio	0.35	0.35	0.35
Impeller inlet to outlet diameter ratio	0.50	0.50	0.50
Impeller outlet blade angle, deg	23.0	23.0	23.0
Injection hole to inducer tip diameter ratio	0.0043	0.0043	0.0043
Injection-hole number	20	20	20
Injection-hole angle from the axis, deg	40	40	40
c/D, front	0.0021	0.0016	0.0011
c/D, rear	0.0020	0.0015	0.0010

Table 2 Head coefficient and efficiency at $1.0Q_d$

	Case 1			Case 2		Case 3	
	Exp.	1-D	CFD [14]	Exp.	1-D	Exp.	1-D
Head coefficient ψ	0.940	0.976	0.936	0.950	0.984	0.967	0.990
Pump total efficiency η	73.3%	73.7%	72.1%	74.1%	75.1%	76.4%	76.8%
Volumetric efficiency η_L	——	91.6%	92.6%	——	93.3%	——	95.6%

of the computation of about 1%, indicating that the 1-D method can predict the performance and the leakage flow rate well. The predicted leakage flow rates are about $4.5\%Q_d$ in each FRS direction for case 1, $3.5\%Q_d$ for case 2, and $2.5\%Q_d$ for case 3. The leakage flow rates through the FRS in the 1-D method were calculated using a simple relation as follows [15]:

$$Q_L = C_f A_{\mathrm{cl}} \sqrt{\left(2\frac{\Delta p}{\rho}\right)}, \qquad C_f = 1 \Big/ \sqrt{f\frac{L_c}{c} + 1.5} \tag{1}$$

Figure 4 shows measured suction performance curves at three flow rates. Suction performance curves of case 2 are not presented in Fig. 4, for a clear comparison between case 1 and case 3. Case 1 shows better suction performance results, although the leakage flow rate (or inducer inlet flow rate) of case 1 is larger than that of case 3. Furthermore, the suction performance improvement seems to increase as the flow rate is decreased. It is well known that the suction performance becomes poor as the inlet flow rate increases. Therefore, it seems that the suction performance becomes better with larger leakage flow rates. Jakobsen [17] noted that the flow injected into the inducer inlet has a favorable effect on the suction performance of the pump and an appropriate amount of the flow injected to the inducer inlet can enhance the suction performance of the pump. The trend that Jakobsen mentioned was found in the present study, although the leakage flow rate difference of $2\%Q_d$ between case 1 and case 3 was seemingly not large enough to affect the suction performance of the inducer.

The computations were performed to investigate the flow structure around the inducer inlet, in which the injected leakage flow interacts with the main flow. The present pump adopts the same configuration as in a previous study [18], with a bearing and strut located upstream of the inducer, as shown in Fig. 1. However, only the inducer with the inlet bearing strut was simulated, instead of the entire pump, and the bearing was simplified as a block to save computational time in the present study.

A commercial 3-D Reynolds-averaged Navier–Stokes method is used in this study [19]. Previous studies using this code showed good agreement with the experiments [14,18]. The method uses an explicit Runge–Kutta scheme and second-order-accurate central-difference scheme with artificial dissipation for integration in time and space. The k-ε turbulence model with an extended wall function is used to simulate turbulence effects. A uniform flow condition is imposed at the inlet. Static pressures are assigned at the outlet of the inducer. Periodic boundary conditions are set at corresponding positions, because only one flow passage is solved for the strut and the inducer. To simulate strut/inducer interaction, a mixing plane [19] is adopted that only allows exchanges of averaged flow properties.

The computational grid that was selected based on the previous study [18] is shown in Fig. 5. Computations are performed both with and without the injected leakage flow at $1.0Q_d$. A leakage flow rate of $3.5\%Q_d$ was imposed for the computation with the injection. Streamline (starting from the injection holes) and surface static pressure distributions with the injection are presented in Fig. 6. The flow structure is very complex near the inducer inlet, due to the backflow and the injected leakage flow interactions. Figure 7 shows circumferentially averaged streamline distributions along the meridional plane with and without the injection. Backflows occur at the inlet of the shroud and become weak when the injection is present.

Figure 8 shows circumferentially averaged absolute-flow-angle distributions at the inducer leading edge. The absolute angles increase from hub to shroud. A prewhirl develops at the inlet, due to the rotation of the inducer blades. The sweepback of the leading edge induces this kind of prewhirl [20]. The strength of the prewhirl (or absolute angle) decreases when an injection is present, indicating that

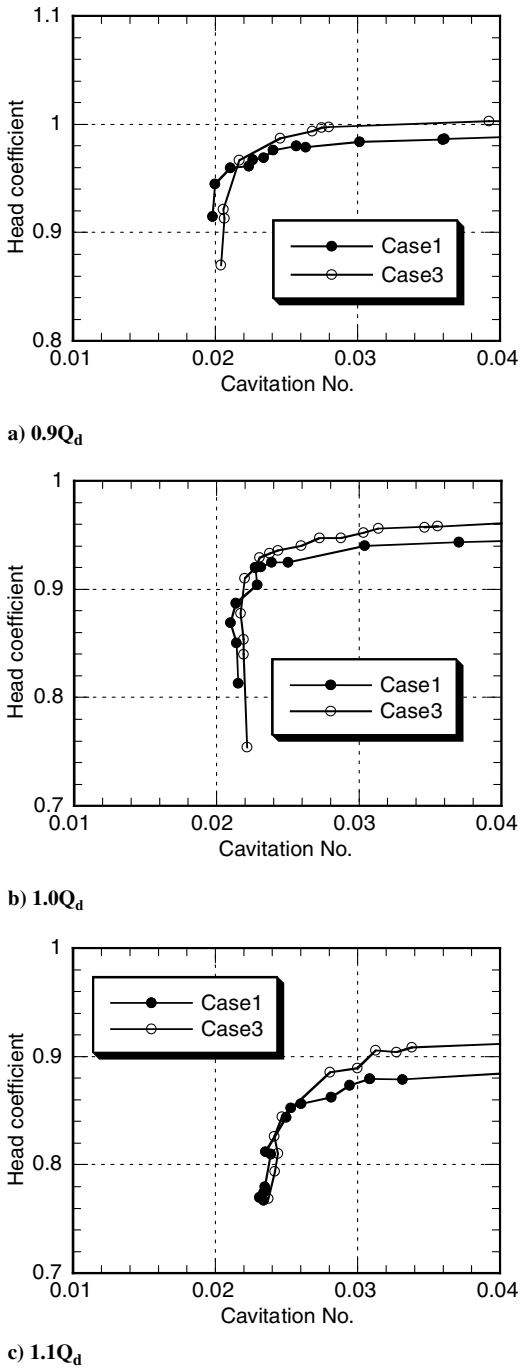

a) $0.9Q_d$

b) $1.0Q_d$

c) $1.1Q_d$

Fig. 4 Measured suction performance curves at three flow rates.

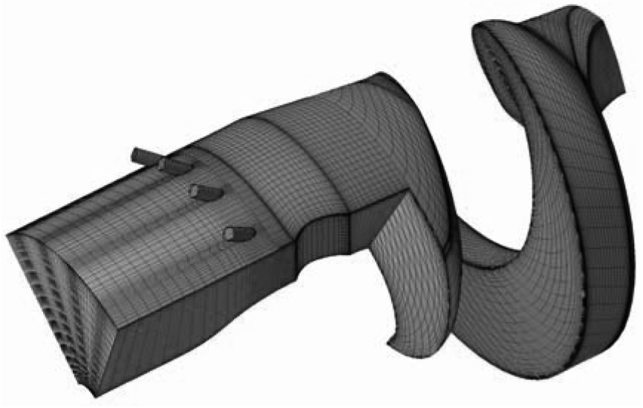

Fig. 5 Computational grid for the calculation (692,793 cells).

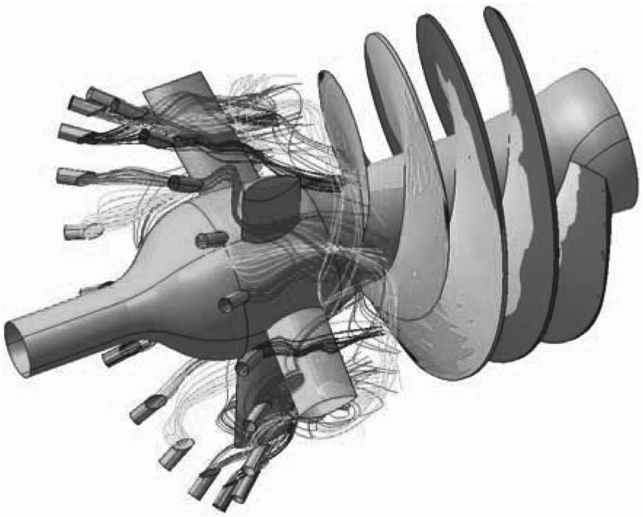

Fig. 6 Streamline and static pressure distributions with injection.

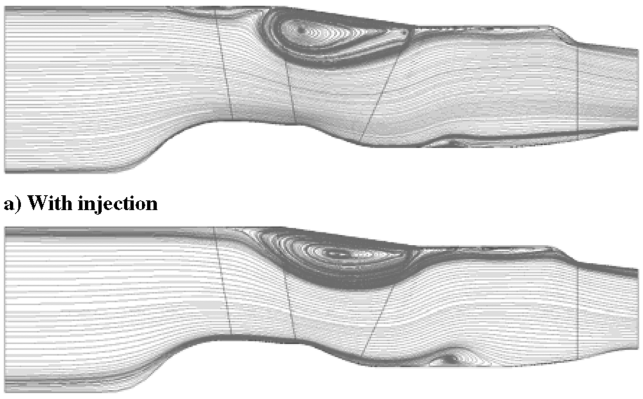

a) With injection

b) Without injection

Fig. 7 Calculated streamline distributions.

the injection prevents the flow from prerotation. Therefore, the injection of the leakage flow into the inlet enhances the suction performance of the pump as the injection prevents backflows from rotating about the axis. This is why the suction performance improvement increases at the lower flow rates, because the backflows become stronger at those flow rates, as shown in Fig. 4. Figure 9 shows circumferentially averaged axial velocity distributions at the inducer leading edge. The axial velocity distribution with the injection is more uniform, due to the weakened backflow.

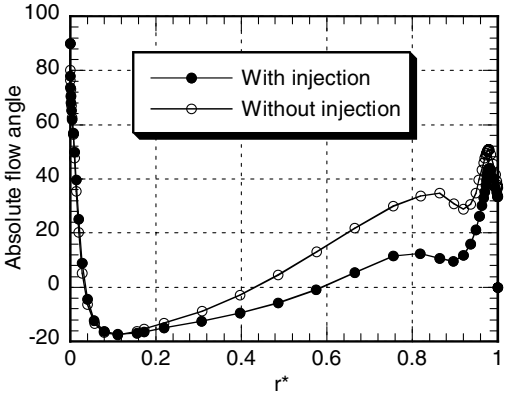

Fig. 8 Calculated absolute-flow-angle distributions.

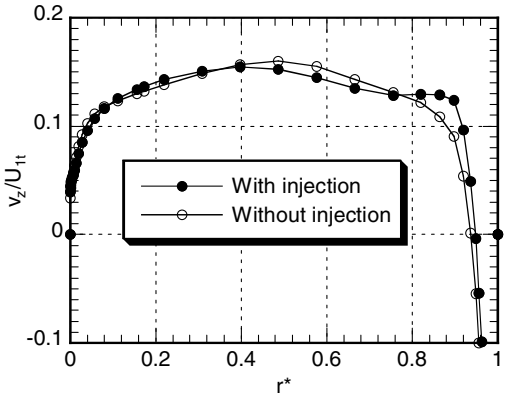

Fig. 9 Calculated axial velocity distributions.

IV. Conclusions

The effects of FRS radial clearance on the performance characteristics of a pump for turbopumps were studied. The overall performance and the suction performance were measured and computations were conducted to investigate leakage flow/inducer interactions. The effects of FRS radial clearance on the performance of a pump are as follows.

1) The head and efficiency of the pump increases when the FRS radial clearance is reduced. The head increases by about 3% and the efficiency increases by about 4% by reducing c/D from 0.0021 to 0.0011 for the front floating ring and 0.0020 to 0.0010 for the rear floating ring.

2) The suction performance of the pump increases when the FRS radial clearance is increased, which may be attributed to the increase of the leakage flow injected to the inducer inlet. The computational results show that the injected leakage flow at the inducer inlet prevents backflows from rotating about the axis, which is presumed to improve the suction performance of the pump by diminishing the size of backflows.

References

[1] Huzel, D. K., and Huang, D. H., *Modern Engineering for Design of Liquid-Propellant Rocket Engines*, AIAA, Washington D.C., 1992, Chap. 6.

[2] Manski, D., Goertz, C., Sabnick, H. D., Hulka, J. R., Goracke, B. D., and Levack, D. J. H., "Cycles for Earth-to-Orbit Propulsion," *Journal of Propulsion and Power*, Vol. 14, No. 5, 1998, pp. 588–604. doi:10.2514/2.5351

[3] Kamijo, K., Yoshida, M., and Tsujimoto, Y., "Hydraulic and Mechanical Performance of LE-7 LOX Pump Inducer," *Journal of Propulsion and Power*, Vol. 9, No. 6, 1993, pp. 819–826. doi:10.2514/3.23695

[4] Lakshminarayana, B., "Fluid Dynamics of Inducers-A Review," *Journal of Fluids Engineering*, Vol. 104, No. 4, 1982, pp. 411–427.

[5] Brennen, C. E., *Hydrodynamics of Pumps*, Concepts ETI, Inc., Norwich, VT, and Oxford Univ. Press, Oxford, 1994.

[6] Shimagaki, M., Kimura, T., Hashimoto, T., Watanabe, M., and Yoshida, Y., "Investigation of Backflow Structure in a Turbopump Inducer with the PIV method," 43rd AIAA/ASME/SAE/ASEE Joint Propulsion Conference and Exhibit, AIAA Paper 2007-5512, July 2007.

[7] Cervone, A., Bramanti, C., Rapposelli, E., Torre, L., and Agostino, L., "Experimental Characterization of Cavitation Instabilities in a Two-Bladed Axial Inducer," *Journal of Propulsion and Power*, Vol. 22, No. 6, 2006, pp. 1389–1395. doi:10.2514/1.19637

[8] Kim, J., Hong, S. S., Jung, E. H., Choi, C. H., and Jeon, S. M., "Development of a Turbopump for a 30 Ton Class Engine," 43rd AIAA/ASME/SAE/ASEE Joint Propulsion Conference and Exhibit, AIAA Paper 2007-5516, July 2007.

[9] Mineo, S., Masataka, N., Kenjiro, K., and Masataka, K., "Research and Development of a Rotating-Shaft Seal for a Liquid Hydrogen Turbopump," *Lubrication Engineering*, Vol. 42, No. 3, 1986, pp. 162–169.

[10] Mamoru, O., Masataka, N., Masataka, K., and Satoshi, H., "Two-Phase Flow in Floating-Ring Seals for Cryogenic Turbopumps," *Tribology Transactions*, Vol. 42, No. 2, 1999, pp. 273–281. doi:10.1080/10402009908982217

[11] Ha, T.-W., Lee, Y.-B., and Kim, C.-H., "Leakage and Rotordynamic Analysis of a High Pressure Floating Ring Seal in the Turbo Pump Unit of a Liquid Rocket Engine," *Tribology International*, Vol. 35, No. 3, 2002, pp. 153–161. doi:10.1016/S0301-679X(01)00110-4

[12] Duan, W., Chu, F., Kim, C.-H., and Lee, Y.-B., "A Bulk-Flow Analysis of Static and Dynamic Characteristics of Floating Ring Seals," *Tribology International*, Vol. 40, No. 3, 2007, pp. 470–478. doi:10.1016/j.triboint.2006.04.010

[13] Hong, S. S., Kim, D. J., Kim, J. S., Choi, C. H., and Kim, J., "Effect of Inducer on Hydraulic Performance of a Turbopump," 41st AIAA/ASME/SAE/ASEE Joint Propulsion Conference and Exhibit, AIAA Paper 2005-2289, July 2005.

[14] Choi, C. H., Noh, J. G., Kim, D. J., Hong, S. S., and Kim, J., "Turbopump Performance Prediction by Using CFD Analysis," Asian Joint Conference on Propulsion and Power 2008, Korea Society of Propulsion Engineers, Paper B6-2, Mar. 2008.

[15] Stepanoff, A. J., *Centrifugal and Axial Flow Pumps*, 2nd ed., Krieger, Malabar, FL, 1957, pp. 182–190.

[16] Japikse, D., Marscher, W. D., and Furst, R. B., *Centrifugal Pump Design and Performance*, Concepts ETI, Inc., Wilder, VT, 1997.

[17] Jakobsen, J. K., "Liquid Rocket Engine Turbopump Inducers," NASA SP-8052, May 1971, pp. 33, 34.

[18] Choi, C. H., Noh, J. G., Kim, J. S., Hong, S. S., and Kim, J., "Effects of a Bearing Strut on the Performance of a Turbopump Inducer," *Journal of Propulsion and Power*, Vol. 22, No. 6, 2006, pp. 1413–1417. doi:10.2514/1.19753

[19] NUMECA Fine/Turbo, Software Package, Ver. 7.1–4, NUMECA International, Brussels, 2006.

[20] Choi, C. H., Kim, J. S., and Kim, J., "Study on the Forward-Sweep Inducer for LRE Turbopumps," 57th International Astronautical Congress, International Astronautical Federation Paper IAC-06-C4.P.1.07, Oct. 2007.

C. Tan
Associate Editor